International Journal of Thermophysics (2020) 41:68
https://doi.org/10.1007/s10765-020-02641-8

ATPC 2019

Thermophysical Properties of a Novel Nanoencapsulated Phase Change Material

Songping Mo[1] · Lijuan He[1] · Lisi Jia[1] · Ying Chen[1] · Zhengdong Cheng[2]

Received: 17 December 2019 / Accepted: 2 March 2020 / Published online: 18 March 2020

Abstract

Thermophysical properties are important parameters that influence the performance of phase change materials (PCMs) and heat transfer fluids. Micro/nanoencapsulation is an effective technique for preventing leakage and enhancing thermophysical properties of PCMs. In the present study, novel D-mannitol nanocapsules with inorganic shells were synthesized as a medium-temperature PCM. The nanocapsulation was confirmed by scanning electronic microscopy. The specific heat and thermal diffusivity of the nanocapsules and their suspension with heat transfer oil as base fluid were measured by a differential scanning calorimeter and light flash apparatus. The thermal conductivity of the nanocapsule suspension was measured using a hot-disk thermal constants analyzer. The viscosity of the nanocapsule suspension was measured by a rotational rheometer. The results show that the thermal conductivity and thermal diffusivity of the nanocapsules were enhanced compared to the bulk of the PCM due to the inorganic shell. The specific heat, thermal conductivity, and viscosity of the nanocapsule suspension were increased compared to the base fluid. The potential of the nanocapsule suspension as a heat storage and transfer fluid was evaluated.

Keywords D-Mannitol · Nanoencapsulation · PCM · Suspension · Thermophysical property

Selected Papers of the 12th Asian Thermophysical Properties Conference.

✉ Ying Chen
chenying@gdut.edu.cn

[1] Guangdong Provincial Key Laboratory on Functional Soft Condensed Matter, School of Materials and Energy, Guangdong University of Technology, Guangzhou 510006, China

[2] Artie McFerrin Department of Chemical Engineering, Texas A&M University, College Station, TX 77843-3122, USA

1 Introduction

Phase change materials (PCMs) are widely used in thermal energy storage for their high energy storage density and constant or narrow temperature variation during energy absorbance and release [1]. Thermal energy storage is an effective way to utilize waste heat by medium-temperature PCMs [2]. Sugar alcohols are medium-temperature PCMs with various advantages, such as high latent heat, non-toxic, and environmentally friendly [3]. Among which D-mannitol (DM) is a sugar alcohol with high latent heat for medium-temperature thermal energy storage [4].

The performance of PCMs is significantly affected by their thermal properties. Encapsulation is effective for enhancing thermophysical properties [5], increasing heat transfer and reducing leakage issues [6]. Salaün *et al.* [7] studied thermal properties of polyurethane microparticles containing xylitol and found that the microparticles could be applied for thermal energy storage. Ma *et al.* [8] studied the influence of core and shell materials and ratios on the thermal properties of micro-PCMs (MPCMs) and revealed that the composition of the core and shell have a great influence on the thermal properties of the MPCMs.

Microcapsules can be added to a base fluid to prepare a suspension called microencapsulated phase change slurry [9], which can be used as a latent functionally thermal fluid [10]. Microcapsule suspensions have remarkable merits, including narrow temperature range and high energy density for thermal energy storage and transfer, compared to traditional fluids. Huang *et al.* [2] reviewed the advances in microcapsule suspensions which have advantages of both the base carrier fluid and the PCM microcapsules, *i.e.*, a significant amount of thermal energy can be stored and transferred by microcapsule suspensions with both good fluidity and high latent heat. The thermal properties of microcapsule suspensions/slurries have been reported in many papers [2]. The thermophysical properties of the suspensions significantly affect their performance; therefore, they are essential for the application of the suspensions.

According to the literature review, the thermophysical properties of microcapsule suspensions are affected by the properties of the microcapsule, which are significantly influenced by the shell materials [11]. In this study, nanoencapsulated D-mannitol (NEDM) was synthesized with SiO_2 shell to enhance the thermophysical properties. The NEDM was dispersed into medium-temperature heat transfer oil to prepare a novel fluid. The thermophysical properties of the NEDM and their suspension were investigated, and the potential of the NEDM suspension as a heat storage and transfer fluid was evaluated, which have not been reported before.

2 Materials and Methods

2.1 Materials

D-Mannitol, tetraethoxysilane (TEOS), and 3-Aminopropyl triethoxysilane (APTS) were purchased from the Aladdin Chemistry Co. Ltd. Cyclohexane (AR, Tianjin Damao chemical reagent company, China) was used as a solvent. Span 80 (Guangzhou Chemical Reagent Company, China) and Tween 80 (Tianjin Fuchen Chemical Reagent Company, China) were used as emulsifiers. Heat transfer oil (Changcheng L-QB300) was used as the base fluid for preparing the NEDM suspension.

2.2 Preparation of NEDM and Its Suspension

The encapsulation based on the sol–gel method is as follows. 15 ml of saturated DM aqueous solution, 65 ml of cyclohexane, 0.1 g of Tween80, and 0.6 g of Span 80 were mixed and stirred for 1.5 h. The mixture was maintained at 50 °C, and 5 ml APTS and 9 ml TEOS were added in drops and stirred mechanically for 8 h. The NEDM was obtained after the product was washed by cyclohexane and freeze dried for 24 h. The NEDM was added to the heat transfer oil and stirred for 30 min to prepare a 2 wt% NEDM suspension.

2.3 Characterization Methods

The morphology of the NEDM was observed through a scanning electron microscope (SEM, SU8010, Hitachi Inc., Japan). The thermophysical properties of pure DM and the NEDM were measured. The specific heat and thermal diffusivity of the NEDM and their suspension were measured by a differential scanning calorimeter (DSC, DSC3 STAR, METTLER TOLEDO, Switzerland) and light flash apparatus (LFA467 HyperFlash HT, Netzsch, Germany). The specific heat measurements were carried out at temperatures from 130 to 200 °C at a heating rate of 10 °C min^{-1}. Thermal conductivity, k, of the NEDM was calculated by

$$k = \alpha \cdot \rho \cdot c \tag{1}$$

where α, ρ, and c are thermal diffusivity, density, and specific heat, respectively. The dispersion stability of the NEDM suspension was measured by Turbiscan Lab^{Expert} (Formulaction, France), an instrument based on the multiple light scattering method, which has been introduced in detail in the literature [12]. The thermal conductivity of the NEDM suspension was measured by a hot-disk thermal constants analyzer (Thermal Constants Analyzer-1500, Hot disk AB, Sweden). The viscosity of the NEDM suspension was measured by a rotational rheometer (Physica MCR301, Austria) at shear rate of 1–100 s^{-1}. The torque resolution of the rheometer was 0.1 nNm.

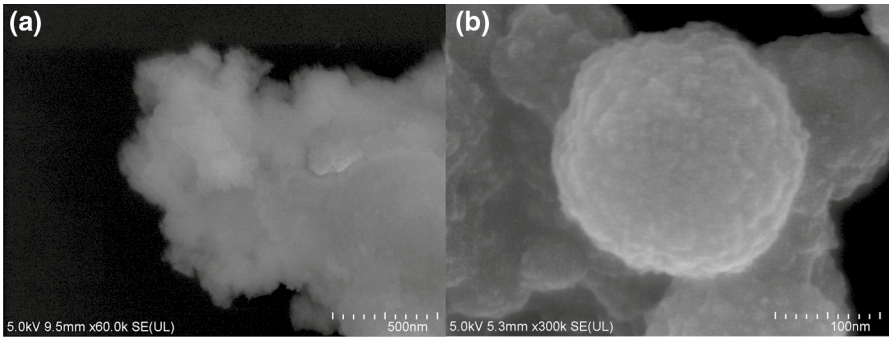

Fig. 1 SEM images of (a) the DM and (b) the NEDM

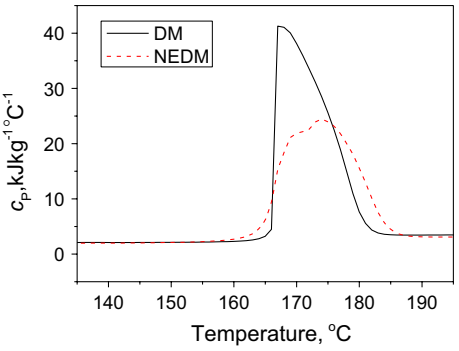

Fig. 2 Specific heat of the DM and the NEDM

The uncertainty of shear stress was 1.7×10^{-3} Pa. The least angular velocity resolution was 10 nrad s^{-1}.

3 Results and Discussion

3.1 Morphology of the DM and NEDM

The morphologies of the DM and the NEDM are shown in Fig. 1. The DM is in a random shape and size (Fig. 1a). By contrast, the NEDM is in the form of spherical particles whose size are in the range of 100–200 nm (Fig. 1b).

3.2 Specific Heat of the DM and NEDM

The specific heat of pure DM and NEDM is presented in Fig. 2. The DM has a peak in the range of 165–185 °C, while the NEDM has a peak in the range of 155–187 °C because of solid–liquid phase change. The maximum specific heats of the DM and NEDM are 41.3 kJ (kg °C)$^{-1}$ and 24.5 kJ (kg °C)$^{-1}$, respectively. The latent heats, which are calculated from the DSC software, are 288.4 kJ kg^{-1}

and 218.9 kJ kg^{-1} for the DM and NEDM, respectively. The decrease in specific heat of the NEDM compared to DM is attributed to the decrease in latent heat. The reason is that phase change does not occur at the SiO_2 shell of the NEDM. Outside the phase change temperature range, the specific heat of the samples is much lower. Below the phase change temperature, the specific heat of the DM is 2.1 kJ (kg °C)$^{-1}$, while that of the NEDM is 2.0 kJ (kg °C)$^{-1}$. Above the phase change temperature, the specific heats of the DM and NEDM are 3.5 kJ (kg °C)$^{-1}$ and 3.1 kJ (kg °C)$^{-1}$, respectively. The higher specific heat above the phase change temperature is higher than that below the phase change temperature for both the DM and NEDM samples. It is because the DM sample and the core of the NEDM sample are in solid and liquid states for temperatures below and above the phase change temperature, respectively; it is well understood that a material in liquid state has higher specific heat than that in its solid state. The specific heat of the NEDM is lower than that of DM because the specific heat of the shell of the NEDM is lower than that of DM. The difference becomes higher above the phase change temperature because DM changes to a liquid state, and its specific heat increases, while the shell of the NEDM remains in a solid state, and its specific heat remains constant.

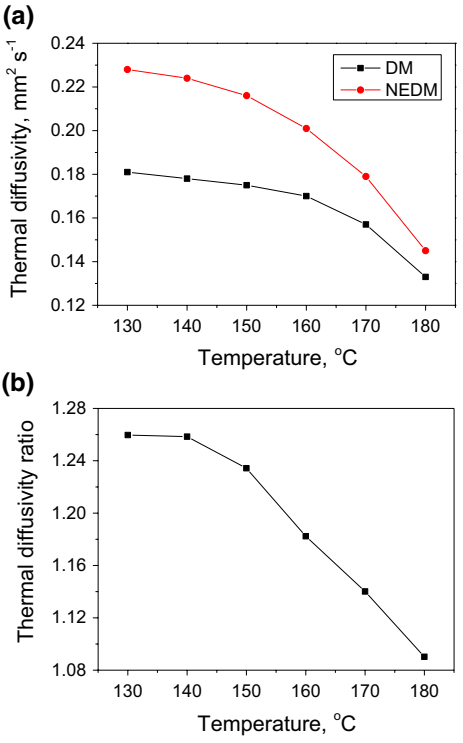

Fig. 3 Thermal diffusivity of DM and NEDM

3.3 Thermal Diffusivity of the NEDM

The thermal diffusivity of the DM and NEDM is shown in Fig. 3. As indicated in Fig. 3a, the thermal diffusivity of NEDM is higher than that of DM at the same temperature. The thermal diffusivity ratio of NEDM to that of DM is defined as

$$r_{\alpha} = \alpha_{\mathrm{NEDM}} / \alpha_{\mathrm{DM}} \tag{2}$$

where α_{NEDM} and α_{DM} are the thermal diffusivities of NEDM and DM, respectively. As indicated in Fig. 3b, the thermal diffusivity of NEDM is more than 108 % of the thermal diffusivity of DM. Both the thermal diffusivity (Fig. 3a) and the thermal diffusivity ratio (Fig. 3b) decrease with increasing temperature. The decrease in thermal diffusivity is relatively slow outside the phase change temperature range; it becomes sharp when the temperature becomes higher than the melting point. These results are consistent with those of studies in the literature, which reported that the thermal diffusivity of a PCM decreases during phase transition [13]. The reason for these results is that the thermal diffusivity of DM in its liquid state is lower than that in its solid state. This is attributed to the shell of the NEDM, which maintains a solid state with a thermal diffusivity higher than that of the liquid-state DM in the studied temperature range.

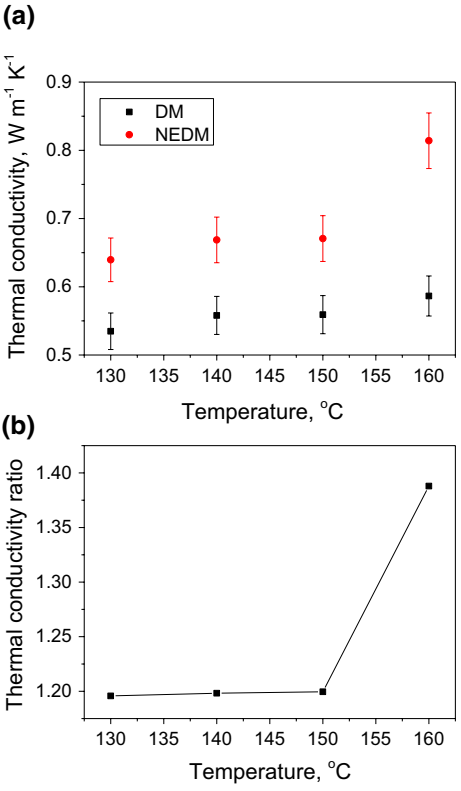

Fig. 4 Thermal conductivity of DM and NEDM

3.4 Thermal Conductivity of the NEDM

Figure 4a shows that the thermal conductivity of the NEDM is higher than that of DM. The thermal conductivity ratio of the NEDM to that of DM is defined as

$$r_{\mathrm{k}} = k_{\mathrm{NEDM}} / k_{\mathrm{DM}} \tag{3}$$

where k_{NEDM} and k_{DM} are thermal conductivity of the NEDM and DM, respectively. As shown in Fig. 4b, the thermal conductivity of NEDM is more than 1.19 times that of the DM. The thermal conductivity enhancement can be attributed to the SiO_2 shell of the NEDM. The thermal conductivity of the SiO_2 shell is 1.296 W m^{-1} K^{-1} [14], which is relatively higher than that of pure DM. It is well understood that the thermal conductivity of NEDM, which is composed of an SiO_2 shell and a DM core, is higher than that of DM. As shown in Fig. 4b, the thermal conductivity ratio does not change significantly with temperature in the 130–150 °C range, but jumps to 1.39 at 160 °C. The reason for this is that the effect of the shell of the NEDM on the thermal conductivity is the same when the DM core is in the solid state. However, the DM core begins to melt at 160 °C, resulting in a higher specific heat (Fig. 2) and consequently a higher thermal conductivity according to Eq. 1. It is worth noting that Eq. 1 may not be appropriate for calculating the thermal conductivity of PCMs in the phase change temperature range. This is because phase change occurs during a specific heat measurement by DSC; however, it may not occur during the short time required for thermal diffusivity measurements conducted by the transient flash method. Therefore, the thermal conductivity value of NEDM at 160 °C may not be adaptable, and the thermal conductivity of samples over 160 °C is not presented in this paper.

3.5 Dispersion Stability of the NEDM Suspension

Figure 5 shows the light transmission and scattering curves of the suspension, where the *x*-axis denotes the height of the sample cell. The results show that within 12 h, the light transmission of the sample remains less than 0.5 %. Meanwhile, the light scattering is less than 4.5 % for the sample at a height of

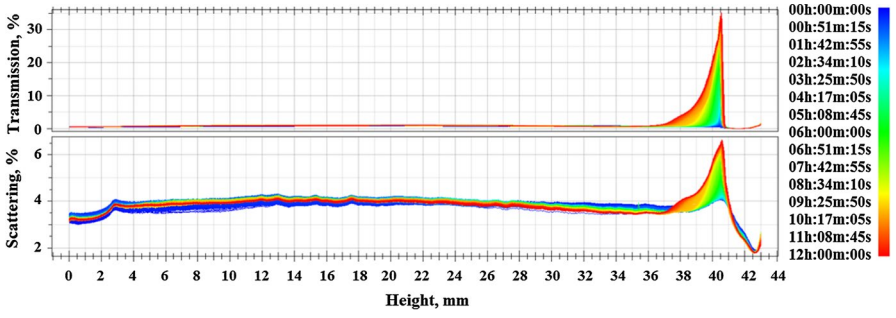

Fig. 5 Dispersion stability of the NEDM suspension

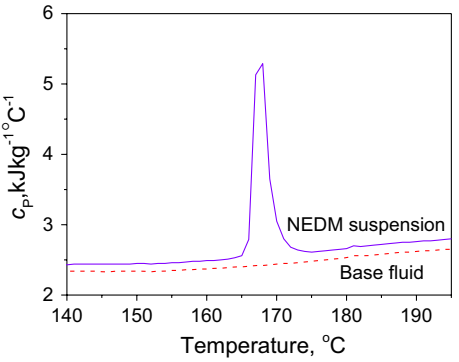

Fig. 6 Specific heat of the base fluid and the NEDM suspension

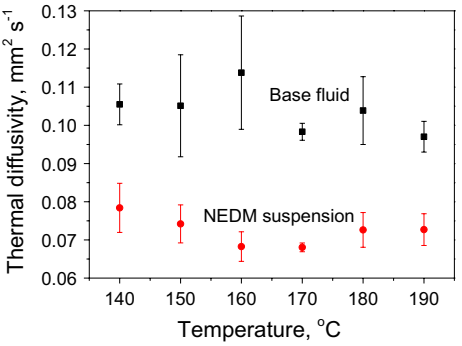

Fig. 7 Thermal diffusivity of the base fluid and the NEDM suspension

0–38 mm of the sample cell. The light transmission and scattering increase at a height of 38–41 mm due to a small NEDM sedimentation portion. The results indicate that the NEDM suspension is relatively stable.

3.6 Specific Heat of the NEDM Suspension

The specific heat of the base fluid and the NEDM suspension are presented in Fig. 6. The specific heat of the base fluid increases from 2.3 kJ (kg °C)$^{-1}$ at 140 °C to 2.6 kJ (kg °C)$^{-1}$ at 190 °C. The specific heat curve of the NEDM suspension exhibits the same tendency as that of the base fluid, except for the peak in the phase change temperature range of the NEDM around 170 °C. The maximum specific heat of the NEDM suspension is 5.3 kJ (kg °C)$^{-1}$, which is 221 % of that of the base fluid. The increase in specific heat of the NEDM suspension is attributed to the PCM core of the NEDM that absorbs heat during the phase change process. The results indicate the promising potential of the NEDM suspension as a heat transfer and thermal energy storage fluid.

3.7 Thermal Diffusivity of the NEDM Suspension

The thermal diffusivities of the base fluid and the NEDM suspension are shown in Fig. 7. The thermal diffusivity of the base fluid is around 0.03 $mm^2\ s^{-1}$ higher than that of the NEDM suspension at the same temperature. This is attributed to the NEDM, which can increase the heat capacity of the base fluid. More thermal energy is required to increase the temperature of the NEDM suspension as the NEDM absorbs thermal energy during measurements. Therefore, the thermal diffusivity of the NEDM suspension is lower compared to the base fluid.

3.8 Thermal Conductivity of the NEDM Suspension

The thermal conductivities of the base fluid and the NEDM suspension are presented in Fig. 8a. The ratio of the thermal conductivity of the NEDM suspension to that of the base fluid is defined as

$$k_{sus}/k_{bf} = 1 + C_k \tag{4}$$

where k_{sus} and k_{bf} are thermal conductivities of the NEDM suspension and the base fluid, respectively. C_k is the enhancement coefficient of thermal conductivity, which

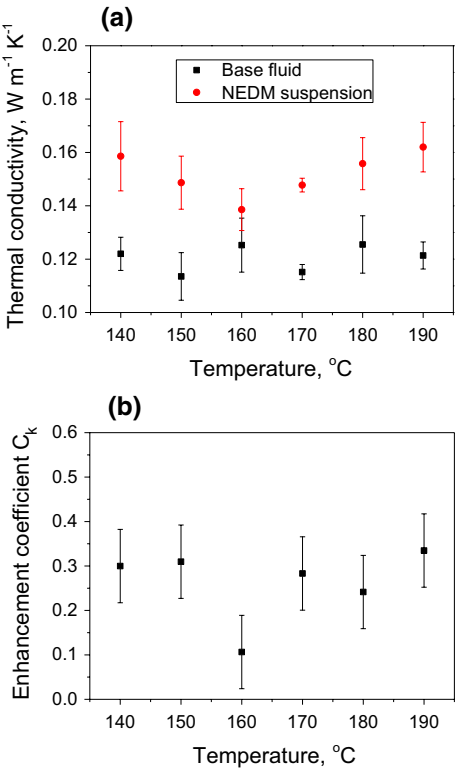

Fig. 8 Thermal conductivity of the base fluid and the NEDM suspension

is plotted in Fig. 8b. The thermal conductivity enhancement coefficient is higher than 10 %. This is because the thermal conductivity of the NEDM is higher than that of the base fluid. The mechanism is the same as that of nanofluids whose thermal conductivities are enhanced by adding nanoparticles with a high thermal conductivity [15].

3.9 Viscosity of the NEDM Suspension

The viscosities of the base fluid and the NEDM suspension as a function of shear rate are shown in Fig. 9. Both the samples exhibit Newtonian behavior, *i.e.*, there is no significant change in viscosity with increasing shear rate (Fig. 9a). The ratio of the viscosity of the NEDM suspension to that of the base fluid is defined as

$$\eta_{\mathrm{sus}} / \eta_{\mathrm{bf}} = 1 + \mathrm{C}_{\eta} \tag{5}$$

where η_{sus} and η_{bf} are viscosities of the NEDM suspension and the base fluid, respectively. C_{η} is the enhancement coefficient of viscosity. As shown in Fig. 9b, the viscosity enhancement coefficient is around 4 %.

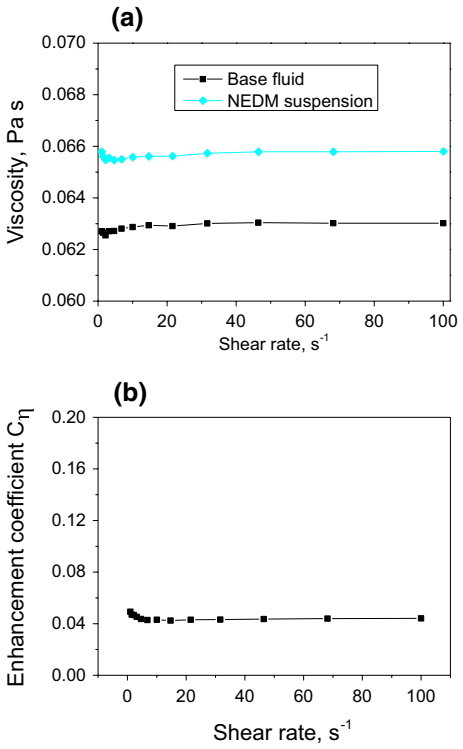

Fig. 9 Viscosity of the base fluid and the NEDM suspension

3.10 Efficiency Evaluation of the NEDM Suspension

The efficiency of a fluid coolant depends on the flow mode. For a fully developed laminar flow, the fluid is beneficial if $C_\eta/C_k < 4$ [16]. The results in Figs. 8 and 9 show that $C_\eta/C_k \sim 0.4$ for the NEDM suspension. This result confirms the high efficiency of the NEDM suspension as a heat transfer fluid.

4 Conclusions

Novel DM nanocapsules and their suspensions with heat transfer oil as a base fluid were prepared and the thermophysical properties were studied. The following conclusions were drawn:

1. The thermal diffusivity and thermal conductivity of the NEDM are more than 8 % and 19 % higher than those of DM in the tested conditions, respectively. This enhancement is due to the improved thermophysical properties and increased heat transfer area by the SiO_2 shell of the NEDM.
2. The specific heat of the NEDM suspension is up to 221 % of the specific heat of the base fluid in the phase change temperature range. The thermal conductivity and viscosity of the NEDM suspension are 10 % and 4 % higher than those of the base fluid, confirming the high efficiency of the NEDM suspension as a heat transfer fluid.
3. The improved thermophysical properties of the NEDM and the NEDM suspension demonstrate their promising potential for application in medium-temperature heat storage and transfer.

Acknowledgments This work was supported by the National Natural Science Foundation of China (Grant Numbers 51976040, 51576050); and the Guangzhou Municipal Science and Technology Project (Grant Number 201704030107). Ying Chen acknowledges the support from the Guangdong Special Support Program (2017TX04N371).

Compliance with Ethical Standards

Conflict of interest The authors declare that they have no conflict of interest.

References

1. J.P. da Cunha, P. Eames, Appl. Energy **177**, 227–238 (2016)
2. X. Huang, C.Q. Zhu, Y.X. Lin, G.Y. Fang, Appl. Therm. Eng. **147**, 841–855 (2019)
3. E.P. del Barrio, A. Godin, M. Duquesne, J. Daranlot, J. Jolly, W. Alshaer, T. Kouadio, A. Sommier, Sol. Energy Mater. Sol. Cells **159**, 560–569 (2017)
4. A. Mojir, N. Grbac, B. Bourke, G. Rosengarten, Sol. Energy Mater. Sol. Cells **176**, 150–156 (2018)
5. C.Y. Zhao, G.H. Zhang, Renew. Sustain. Energy Rev. **15**, 3813–3832 (2011)

6. A. Arshad, M. Jabbal, Y.Y. Yan, J. Darkwa, Int. J. Energy Res. **43**, 5572–5620 (2019)
7. F. Salaun, G. Bedek, E. Devaux, D. Dupont, D. Deranton, Int. J. Thermophys. **30**, 1242–1256 (2009)
8. Y.H. Ma, Q.F. Xie, X.Z. Wang, J. Appl. Polym. Sci. **136**, 47777 (2019)
9. L. Yang, S.L. Liu, H.F. Zheng, Renew. Sustain. Energy Rev. **114**, 109312 (2019)
10. K. Dutkowski, J.J. Fiuk, Int. J. Heat Mass Transf. **134**, 1209–1217 (2019)
11. M. Jurkowska, I. Szczygiel, Appl. Therm. Eng. **98**, 365–373 (2016)
12. S.P. Mo, Z.W. Liu, X. Yuan, Y. Chen, L.S. Jia, Z. Yang, T. Yin, Z.D. Cheng, Nanosci. Nanotech. Lett. **9**, 1505–1513 (2017)
13. H.Y. Chen, Z.M. Yue, D.D. Ren, H.R. Zeng, T.R. Wei, K.P. Zhao, R.G. Yang, P.F. Qiu, L.D. Chen, X. Shi, Adv. Mater. **31**, 1086518 (2019)
14. H.Z. Zhang, X.D. Wang, D.Z. Wu, J. Colloid Interf. Sci. **343**, 246–255 (2010)
15. S. Eiamsa-ard, K. Kiatkittipong, Int. J. Thermophys. **40**, 28 (2019)
16. E.V. Timofeeva, J.L. Routbort, D. Singh, J. Appl. Phys. **106**, 014304 (2009)